Chapter II: Dip-Moveout for Depth-Variable Velocity

2.1. Approximations for Depth-Variable Velocity

The derivation of dip-moveout (DMO) by Fourier transform in chapter I is based on the assumption that velocity is constant. Although this assumption is almost never valid, the application to recorded data included in chapter I suggests that applying constant-velocity DMO is probably better than applying no DMO at all. A similar statement could as well be made about normal-moveout (NMO) correction: NMO assuming a constant velocity is probably better than omitting NMO entirely. In practice, of course, velocity is rarely assumed to be constant in applying NMO. Even though exact traveltime equations for variable-velocity media are difficult (or impossible) to obtain, good approximations of these equations make the constant-velocity assumption unnecessary.

This chapter addresses the questions of (1) how DMO by Fourier transform may be modified to approximately handle depth-variable velocity, and (2) whether or not the modification is worthwhile. The Fourier transform over common-midpoint (CMP) y in the DMO equations (1.12) precludes a simple modification to cope with lateral velocity variations. Lateral velocity variations are more appropriately dealt with in the untransformed y domain, perhaps using a finite-difference DMO algorithm as discussed by Yilmaz and Claerbout (1980). In this chapter, velocity is assumed to vary only with depth.

Taner and Koehler (1969) showed that NMO correction for depth-variable velocity may be based on the following traveltime equation:

$$t^2 = t_n^2 + \frac{4h^2}{V_2^2(t_n)} + O(h^4) \ , \qquad (2.1a)$$

where t is recording time, t_n is NMO time, h is half-offset, and $V_2(t_n)$ is the root-mean-square (RMS) velocity function defined by

$$V_2^2(t_n) \equiv \frac{1}{t_n}\int_0^{t_n} ds\, v^2(s) \quad . \tag{2.1b}$$

The RMS velocity V_2 and the interval velocity v are defined to be functions of migrated, two-way vertical time; but, for the horizontal reflectors assumed by Taner and Koehler, migrated time is the same as NMO time t_n. Dropping the $O(h^4)$ terms in equation (2.1a), NMO correction is defined by the following transformation from recorded seismograms $p(t,y,h)$ to NMO-corrected seismograms $p_n(t_n,y,h)$:

$$p_n(t_n,y,h) \equiv p[\sqrt{t_n^2 + 4h^2/V_2^2(t_n)},y,h] \quad . \tag{2.2}$$

Equations (2.1) are appropriate only for horizontal reflectors. Shah (1973) provided the following generalization of these equations for dipping reflectors:

$$t^2 = t_0^2 + \frac{4h^2}{V_{NMO}^2(t_m)} + O(h^4) \quad , \tag{2.3a}$$

where t_0 denotes zero-offset time, t_m denotes migrated (two-way vertical) time, and V_{NMO} is defined by

$$V_{NMO}^2(t_m) \equiv \frac{1}{t_0}\int_0^{t_m} \frac{ds\, v^2(s)}{[1-\lambda^2 v^2(s)]^{3/2}} \quad . \tag{2.3b}$$

Zero-offset time t_0 and migrated time t_m are related by

$$t_0 = \int_0^{t_m} \frac{ds}{[1-\lambda^2 v^2(s)]^{1/2}} \quad , \tag{2.3c}$$

and λ in both equations (2.3b) and (2.3c) is defined by

$$\lambda \equiv \frac{\sin\theta}{v(0)} = \frac{1}{2}\frac{\Delta t_0}{\Delta y} = \frac{1}{2}\frac{k}{\omega_0} \quad . \tag{2.3d}$$

θ denotes the emergence angle of the zero-offset ray. As indicated by equation (2.3d), this angle is related to the slope of the corresponding reflection in a zero-offset section; and this slope, in turn, corresponds to a wavenumber-frequency ratio after Fourier transformation. Figure 1 illustrates the raypaths corresponding to each of the traveltimes t, t_0, and t_m in equations (2.3).

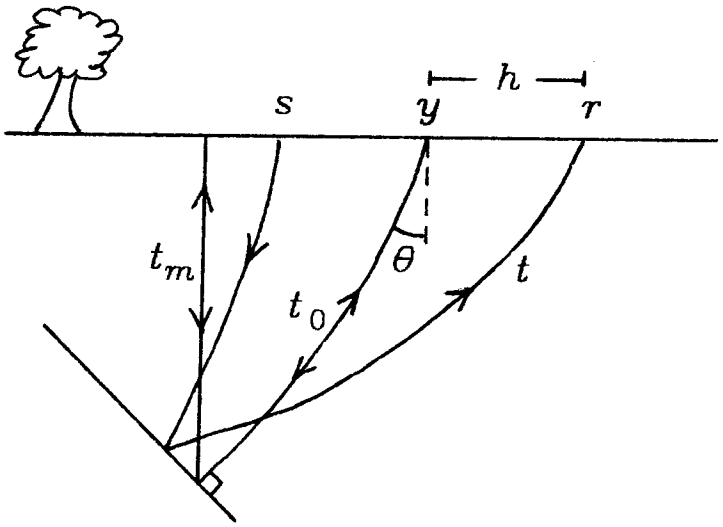

FIG. 2.1. Several raypaths for depth-variable velocity. Each traveltime in equations (2.3) is associated with a particular raypath. The time to propagate along the non-zero-offset raypath is recording time t, the time to propagate along the zero-offset raypath is t_0, and the vertical raypath corresponds to migrated (two-way vertical) time t_m.

That equations (2.3) are correct in general is hardly obvious, but one can easily verify that they are correct for two special cases. First, note that if $v(t_m) = v = constant$, then

$$1 - \lambda^2 v^2 = \cos^2\theta \ ,$$

$$t_0 = \frac{t_m}{\cos\theta} \ ,$$

$$V^2_{NMO}(t_m) = \frac{v^2}{\cos^2\theta} \ ,$$

and equation (2.3a) reduces to the dip-corrected NMO equation (1.3) of chapter I, which is correct for constant-velocity. Second, if $\theta = 0$, then $t_0 = t_m$ and $V_{NMO}(t_m) = V_2(t_m)$; and equations (2.3) reduce to equations (2.1), which are correct for horizontal reflectors. The proof of the general case may be found in Shah's (1973) paper.

Using equation (2.1a) and dropping $O(h^4)$ terms, equation (2.3a) may be rewritten as a transformation from NMO time t_n to zero-offset time t_0:

$$t_0^2 = t_n^2 + \left[\frac{1}{V_2^2(t_n)} - \frac{1}{V_{NMO}^2(t_m)}\right] 4h^2 \quad . \tag{2.4}$$

Recalling from chapter I the Fourier transform of a zero-offset section,

$$P_0(\omega_0,k,h) = \int dt_0\, e^{i\omega_0 t_0} \int dy\, e^{-iky}\, p_0(t_0,y,h) \quad ,$$

equation (2.4) may be used (as in chapter I) to change the integration over t_0 to an integration over t_n; the result is

$$P_0(\omega_0,k,h) = \int dt_n\, A^{-1}\, e^{i\omega_0 t_n A} \int dy\, e^{-iky}\, p_n(t_n,y,h) \quad , \tag{2.5a}$$

where

$$A = A(t_n,\omega_0,h,k) \equiv \left\{1 + \left[\frac{1}{V_2^2(t_n)} - \frac{1}{V_{NMO}^2(t_m)}\right] \frac{4h^2}{t_n^2}\right\}^{1/2} \quad . \tag{2.5b}$$

(All velocity gradients have been ignored in deriving the Jacobian A^{-1} of the change of variable.) The inverse Fourier transform of $P_0(\omega_0,k,h)$ yields the desired

$$p_0(t_0,y,h) = \frac{1}{4\pi^2} \int d\omega_0\, e^{-i\omega_0 t_0} \int dk\, e^{iky}\, P_0(\omega_0,k,h) \quad . \tag{2.5c}$$

Equations (2.5) transform NMO-corrected seismograms $p_n(t_n,y,h)$, which are defined by equation (2.2), to zero-offset seismograms $p_0(t_0,y,h)$. As written,

equations (2.5) would be difficult to implement, because of the complicated dependence of $V_{NMO}(t_m)$ on ω_0 and k, and also because $V_{NMO}(t_m)$ depends on migrated time t_m instead of on NMO time t_n. The latter dependence should have been eliminated in the change of integration variable from t_0 to t_n, but it remains because equation (2.4) cannot be analytically solved for t_0 in terms of t_n. The complicated dependence on ω_0 and k (actually k/ω_0) may be simplified by approximating equation (2.3b) for small λ:

$$V_{NMO}^2(t_m) = \frac{t_m}{t_0}\left[V_2^2(t_m) + \frac{3\lambda^2}{2}V_4^4(t_m)\right] + O(\lambda^4) , \qquad (2.6)$$

where $V_4(t_m)$ is defined by

$$V_4^4(t_m) \equiv \frac{1}{t_m}\int_0^{t_m} ds\, v^4(s) .$$

A similar approximation for t_0,

$$t_0 = t_m\left[1 + \frac{\lambda^2}{2}V_2^2(t_m)\right] + O(\lambda^4) , \qquad (2.7)$$

enables one to approximate equation (2.4) as

$$t_0^2 \approx t_n^2 + \left\{\frac{1}{V_2^2(t_n)} - \frac{1}{V_2^2(t_m)} + \left[\frac{3\,V_4^4(t_m)}{2\,V_2^4(t_m)} - \frac{1}{2}\right]\lambda^2\right\}4h^2 . \qquad (2.8)$$

Like equation (2.4), equation (2.8) cannot be solved analytically for t_0 in terms of t_n; however, the dependence on t_m may be removed by using a truncated Taylor series approximation

$$\frac{1}{V_2^2(t_m)} \approx \frac{1}{V_2^2(t_n)} - \frac{2(t_m - t_n)\,V_2'(t_n)}{V_2^3(t_n)} ,$$

where $V_2'(t_n)$ denotes the derivative of the RMS velocity function. After discarding

all $O(h^4)$ and $O(\lambda^4)$ terms, equation (2.8) becomes

$$t_0^2 \approx t_n^2 + \left[\frac{3V_4^4(t_n)}{2V_2^4(t_n)} - \frac{1}{2} - \frac{t_n V_2'(t_n)}{V_2(t_n)}\right] 4\lambda^2 h^2 \quad . \tag{2.9}$$

Using equation (2.9) instead of equation (2.4) to define a change of variable from t_0 to t_n yields equations (2.5), but with $A(t_n,\omega_0,h,k)$ approximated by

$$A(t_n,\omega_0,h,k) \approx \left\{1 + \left[\frac{3V_4^4(t_n)}{2V_2^4(t_n)} - \frac{1}{2} - \frac{t_n V_2'(t_n)}{V_2(t_n)}\right] \frac{k^2h^2}{\omega_0^2 t_n^2}\right\}^{1/2} \quad . \tag{2.10}$$

Equations (2.5a), (2.5c), and (2.10) provide a practical algorithm for applying approximate DMO correction for depth-variable velocity. This algorithm will be referred to simply as *new*, and the algorithm implied by equations (1.12) of chapter I will be referred to as *old*. Table 2.1 summarizes both the old and new algorithms.

Old (Constant-Velocity) and New (Depth-Variable-Velocity) DMO	
Old	$A(t_n,\omega_0,h,k) = \left(1 + \frac{k^2h^2}{\omega_0^2 t_n^2}\right)^{1/2}$
New	$A(t_n,\omega_0,h,k) = \left\{1 + \left[\frac{3V_4^4(t_n)}{2V_2^4(t_n)} - \frac{1}{2} - \frac{t_n V_2'(t_n)}{V_2(t_n)}\right] \frac{k^2h^2}{\omega_0^2 t_n^2}\right\}^{1/2}$
Both	$P_0(\omega_0,k,h) = \int dt_n\, A^{-1}\, e^{i\omega_0 t_n A} \int dy\, e^{-iky}\, p_n(t_n,y,h)$ $p_0(t_0,y,h) = \frac{1}{4\pi^2}\int d\omega_0\, e^{-i\omega_0 t_0} \int dk\, e^{iky}\, P_0(\omega_0,k,h)$

TABLE 2.1. The difference between the old DMO algorithm and the new DMO algorithm lies only in the definition of the function $A(t_n,\omega_0,h,k)$. The new algorithm approximately handles velocity variations with depth; the approximation is best when velocity gradients are small. Note that the new algorithm reduces to the old algorithm when velocity is constant.

An attractive feature of the new DMO algorithm is that it becomes equivalent to the old algorithm when velocity is constant. Therefore, in spite of the numerous approximations made in deriving the new algorithm, one can expect it to be quite accurate, even for large offsets and steep dips, if velocity gradients are small. The approximations may certainly be improved, but only at the cost of substantially complicating the new algorithm. Given a computer program based on the old algorithm, the modifications required to implement the new algorithm in Table 2.1 are trivial. What is perhaps more important is that the computational cost of this new algorithm is essentially no greater than that of the old algorithm, because the velocity-dependent factors required by the new algorithm need be computed only once.

2.2. Application to Synthetic Data

To test the new DMO algorithm, synthetic seismograms were computed assuming a linear increase in velocity with depth for a subsurface containing only four point scatterers. The synthetic zero-offset section is plotted in Figure 2.2a, and several CMP gathers are plotted in Figure 2.2b. The goal in NMO and DMO processing is to make the non-zero-offset traces in the CMP gathers resemble the zero-offset traces. The zero-offset section may be thought of as an ideal CMP stack of NMO- and DMO-corrected traces.

The synthetic traces are accurate only with respect to analytically computed reflection times. No attempt has been made to model amplitude effects. The important parameters used in computing the synthetic traces follow:

Surface velocity	1.5 km/sec
Velocity gradient	0.6 sec^{-1}
CMP interval	0.033 km
Offset interval	0.133 km

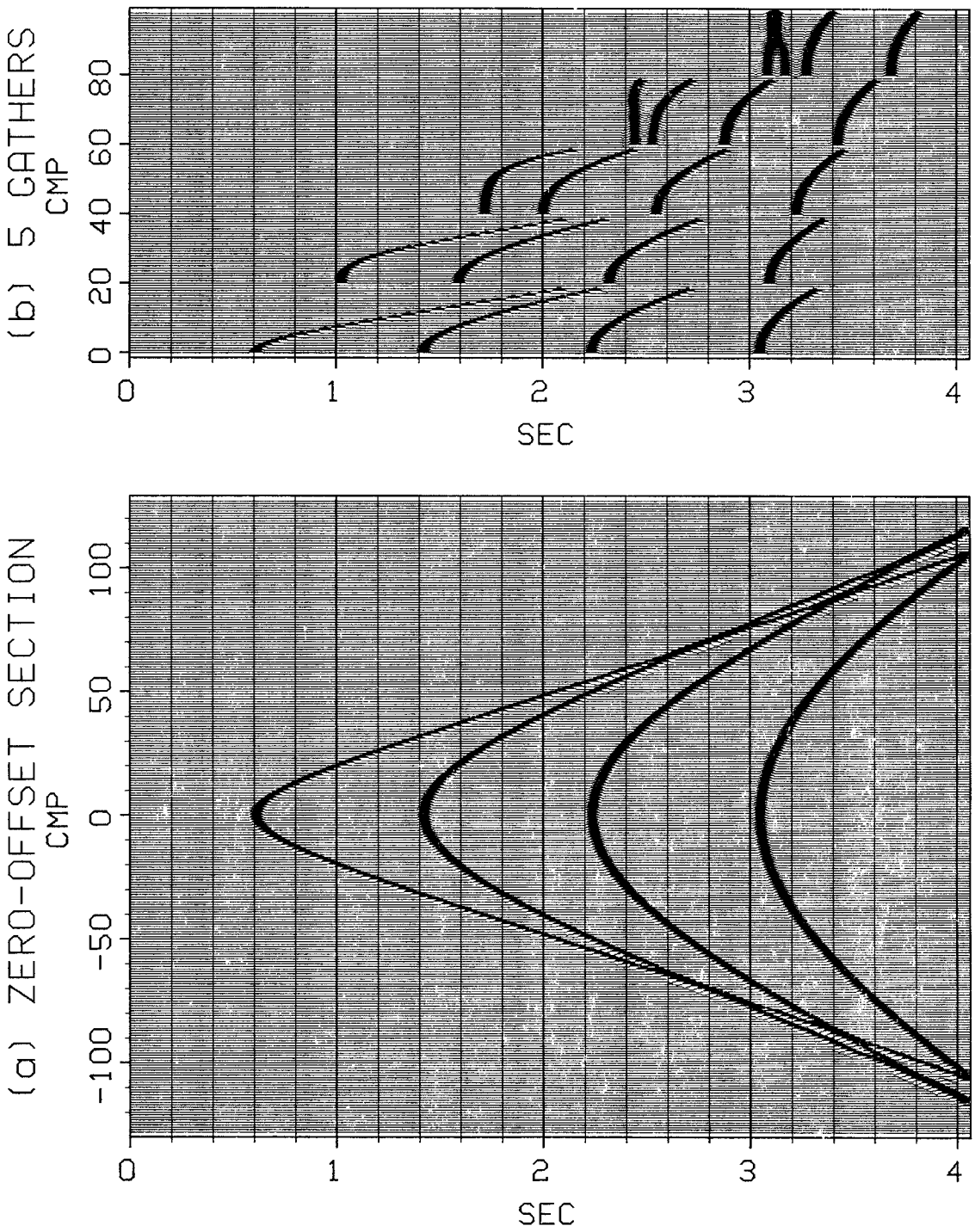

FIG. 2.2. (a) Synthetic zero-offset section and (b) five CMP gathers for a subsurface model consisting of four point scatterers. Velocity was assumed to increase linearly with depth. Note in (b) the familiar (almost hyperbolic) moveout trajectories at CMP 0, where the scatterers are located; these trajectories are distorted at CMP locations farther from the scatterers. The zero-offset section plotted in (a) may be thought of as an ideal CMP stack, after NMO and DMO correction, of traces such as those plotted in (b).

Minimum offset	0 km
Maximum offset	3.325 km
Offsets per CMP	26

These parameters were chosen to approximate those for the recorded data of chapter I. Velocity as a function of depth is plotted in Figure 2.3a, and the corresponding RMS velocity as a function of migrated time is plotted in Figure 2.3b.

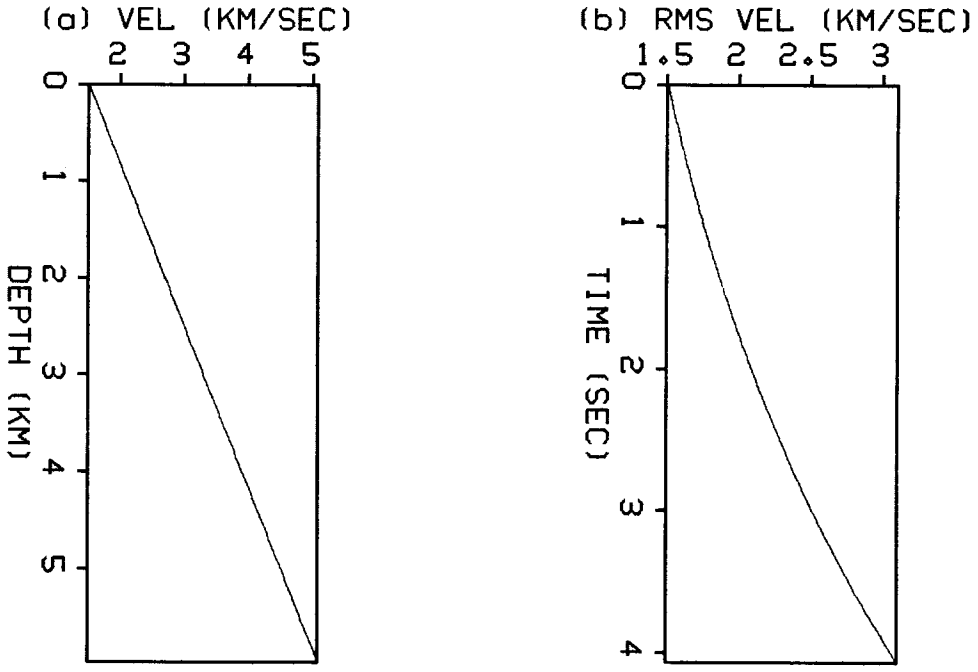

FIG. 2.3. (a) Velocity as a linear function of depth and (b) the corresponding RMS velocity as a (nonlinear) function of migrated (two-way vertical) time. The surface velocity (1.5 km/sec) and the velocity gradient (0.6 sec^{-1}) were chosen to yield RMS velocities roughly approximating those estimated for the recorded data of chapter I.

The synthetic traces were processed by first applying NMO correction, using equation (2.2) and the RMS velocity function of Figure 2.3b. Then, after applying the new DMO transformation of Table 2.1 to each constant-offset section, the CMP stack was computed. This stack, which is plotted in Figure 2.4a, should be compared with the zero-offset section (the ideal CMP stack) plotted in Figure 2.2a. (The CMP stack in Figure 2.4a has been normalized by the number of offsets summed, so that a direct comparison with Figure 2.2a is valid.) The most obvious difference between the two stacks is in the amplitude of the earliest diffraction. The weakness of this diffraction in Figure 2.4a is due to misalignment of the corresponding event in the unstacked CMP gathers. Five such NMO- and DMO-corrected gathers are plotted in Figure 2.4b.

To determine whether or not any advantage exists in using the new algorithm, the above test was repeated using the old DMO algorithm. The resulting CMP stack, plotted in Figure 2.5a, should be compared with that of Figure 2.4a. Note that the limbs of the earliest diffractions are weaker in Figure 2.5a than in Figure 2.4a. Comparison of the five CMP gathers plotted in Figure 2.5b with those plotted in Figure 2.4b reveals that the limbs of the diffractions are less well aligned by the old DMO algorithm than by the new algorithm. For this synthetic test, the new algorithm yields a CMP stack significantly better than that obtained with the old algorithm.

The CMP stack computed using either the new or old DMO algorithm is significantly better than that computed without any DMO correction. The CMP stack of traces without DMO correction is plotted in Figure 2.6a, and five NMO-corrected (only) CMP gathers are plotted in Figure 2.6b. NMO correction based on equation (2.2) is sufficient for CMP 0, where the zero-offset slope of the diffractions is zero. For other CMPs, however, where the zero-offset slope is non-zero, DMO correction by either the new or old algorithm is necessary to reduce the overcorrection of traces seen in Figure 2.6b.

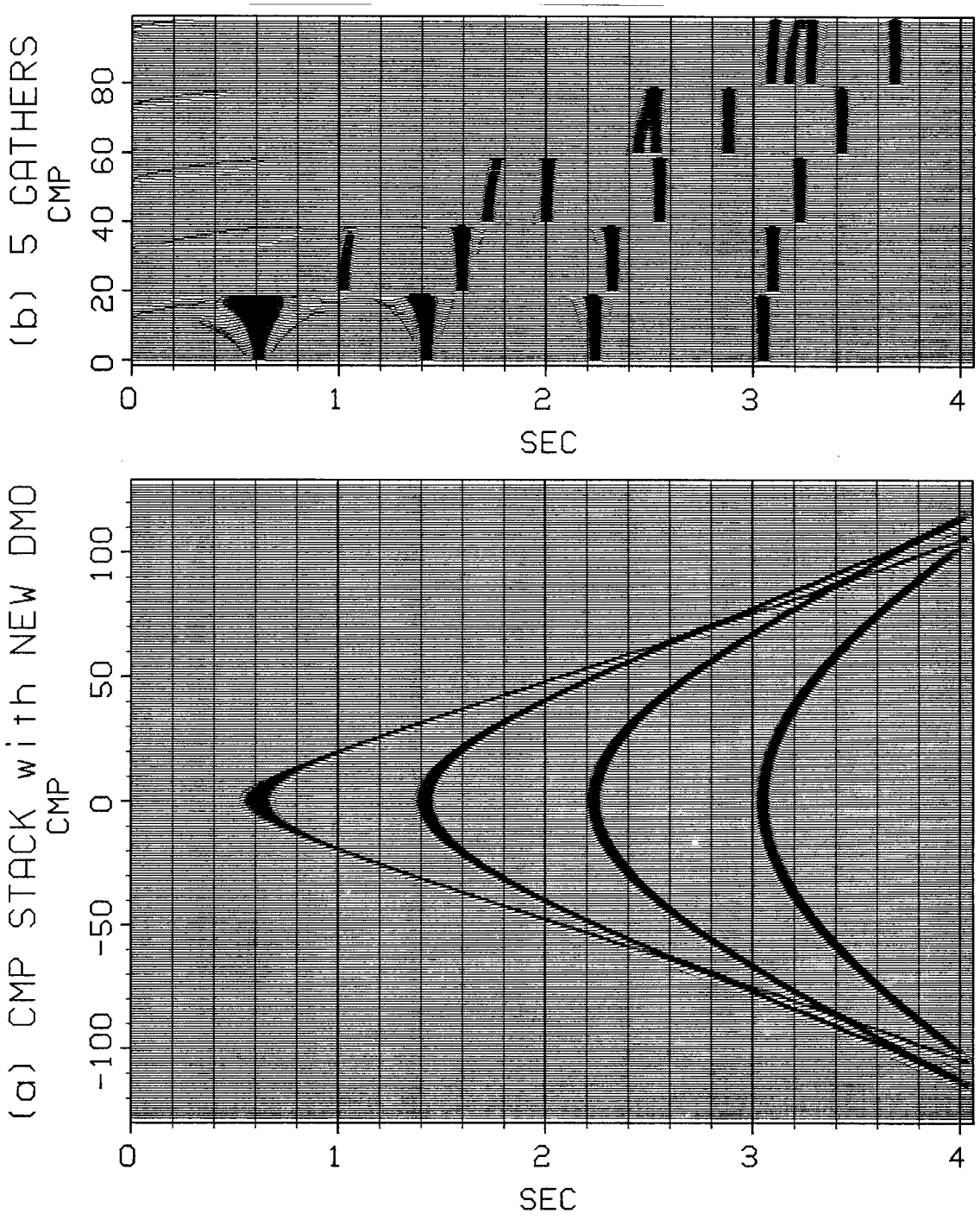

FIG. 2.4. (a) CMP stack computed using the new DMO algorithm of Table 2.1 and (b) five CMP gathers of unstacked, NMO- and DMO-corrected traces. The stack has been normalized by the number of offsets summed to enable comparison with the zero-offset section (ideal stack) plotted in Figure 2.2a. The quality of the stack depends on the alignment of events in the unstacked traces. The alignment of early events in Figure 2.4b is poor due to approximations made in deriving the new DMO algorithm, but compare the stack plotted in Figure 2.4a with that in Figure 2.5a to see the advantage in using the new algorithm instead of the old.

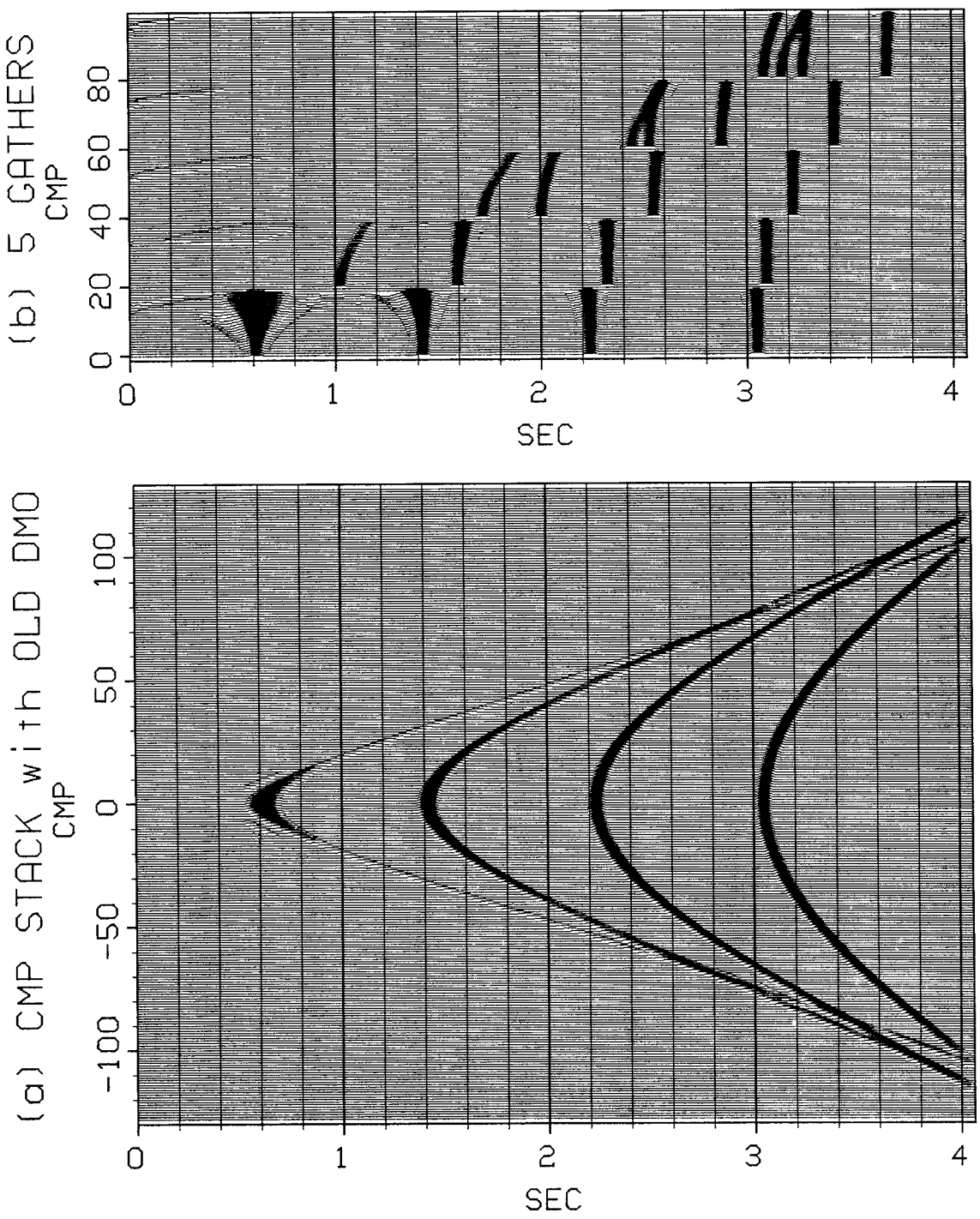

FIG. 2.5. (a) CMP stack computed using the old DMO algorithm of Table 2.1 and (b) five CMP gathers of unstacked, NMO- and DMO-corrected traces. The undercorrection of traces seen in the CMP gathers is due to the increase in velocity with depth, which was ignored in deriving the old algorithm. Compare the CMP stack in (a) with that plotted in Figure 2.4a; the latter was computed using the new DMO algorithm.

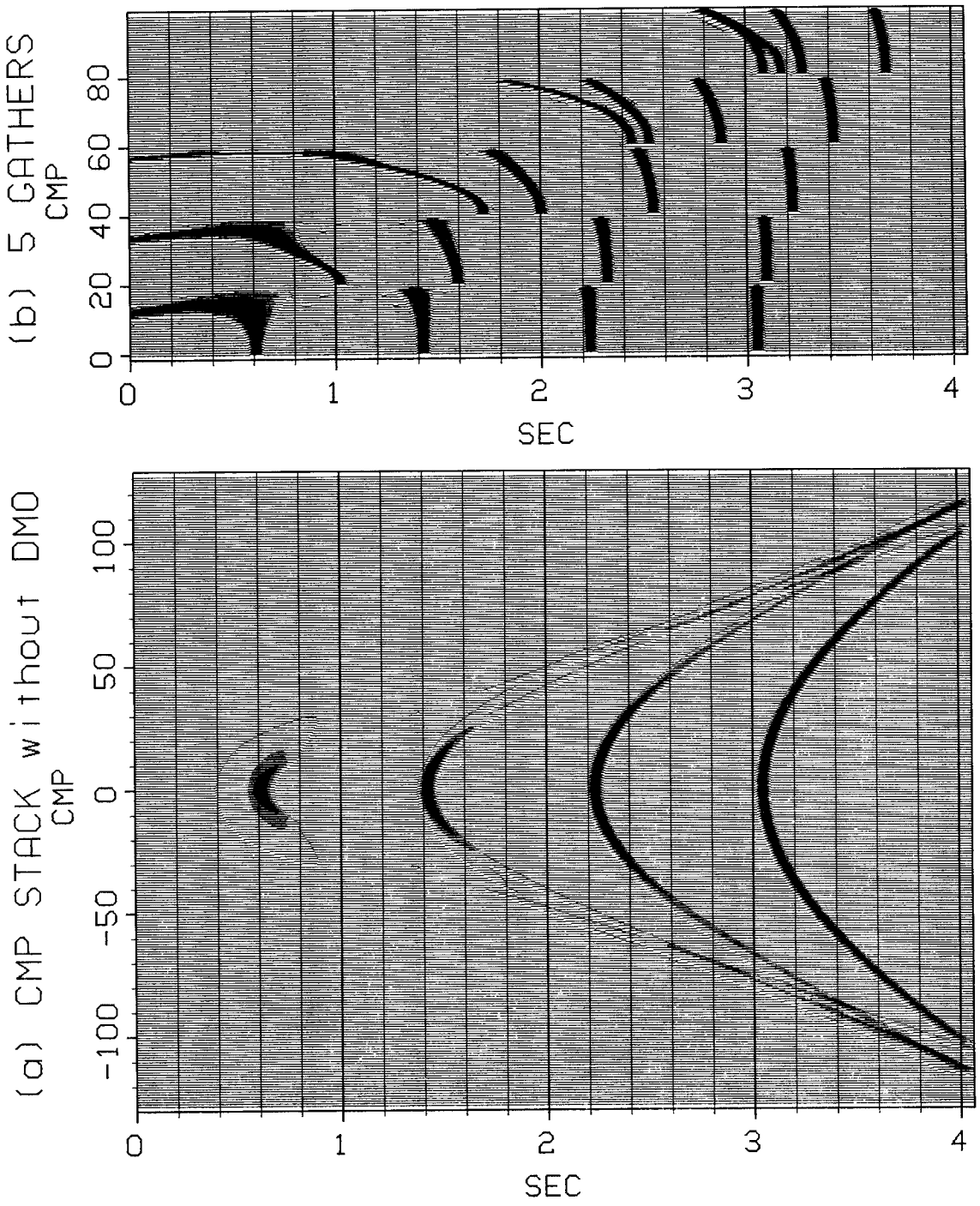

FIG. 2.6. (a) CMP stack computed using only NMO correction and (b) five CMP gathers of unstacked, NMO-corrected traces. NMO correction alone is sufficient only near CMP 0, where the slope of the diffractions (as measured on the zero-offset section) is zero. DMO correction, by either the new or old algorithm, is required at other CMPs (where the zero-offset slope is non-zero) to reduce the gross overcorrection of traces seen in (b).

2.3. Application to Seismic Data

If the DMO process is thought of as a first-order correction to conventional NMO and stack processing, then the application to synthetic data in the previous section suggests that the modification of DMO to approximately handle depth-variable velocity is only a second-order correction. The relative importance of these corrections is further illustrated by application of the new DMO algorithm to the recorded data discussed in chapter I. Plotted in Figure 2.7a is a CMP stack of the recorded data, computed using the new DMO algorithm of Table 2.1. For comparison, the CMP stack obtained using the old DMO algorithm is replotted (from Figure 1.10a of chapter I) in Figure 2.7b. Except for the differences in the DMO algorithms given in Table 2.1, the processing used to obtain these CMP stacks was identical.

The stacks in Figures 2.7a and 2.7b are very similar. The difference, computed by subtracting the stack in Figure 2.7b from that in Figure 2.7a, is plotted in Figure 2.7c. This difference should be compared with that plotted in Figure 1.10c of chapter I, which is the difference between including and omitting (old) DMO correction in the processing sequence. Compared with the improvement obtained by DMO correction in the first place, the additional improvement obtained by modifying the DMO algorithm for depth-variable velocity appears insignificant for these recorded data. Improvements in prestack processing were also insignificant. In particular, velocity estimates obtained after applying the new DMO algorithm were virtually identical to those obtained with the old algorithm.

2.4. Summary

DMO by Fourier transform may be easily modified to approximately handle depth-variable velocity. The new DMO algorithm given in Table 2.1 represents a useful compromise between computational efficiency and accuracy. By avoiding some of the approximations made in deriving this algorithm, more accurate algorithms for

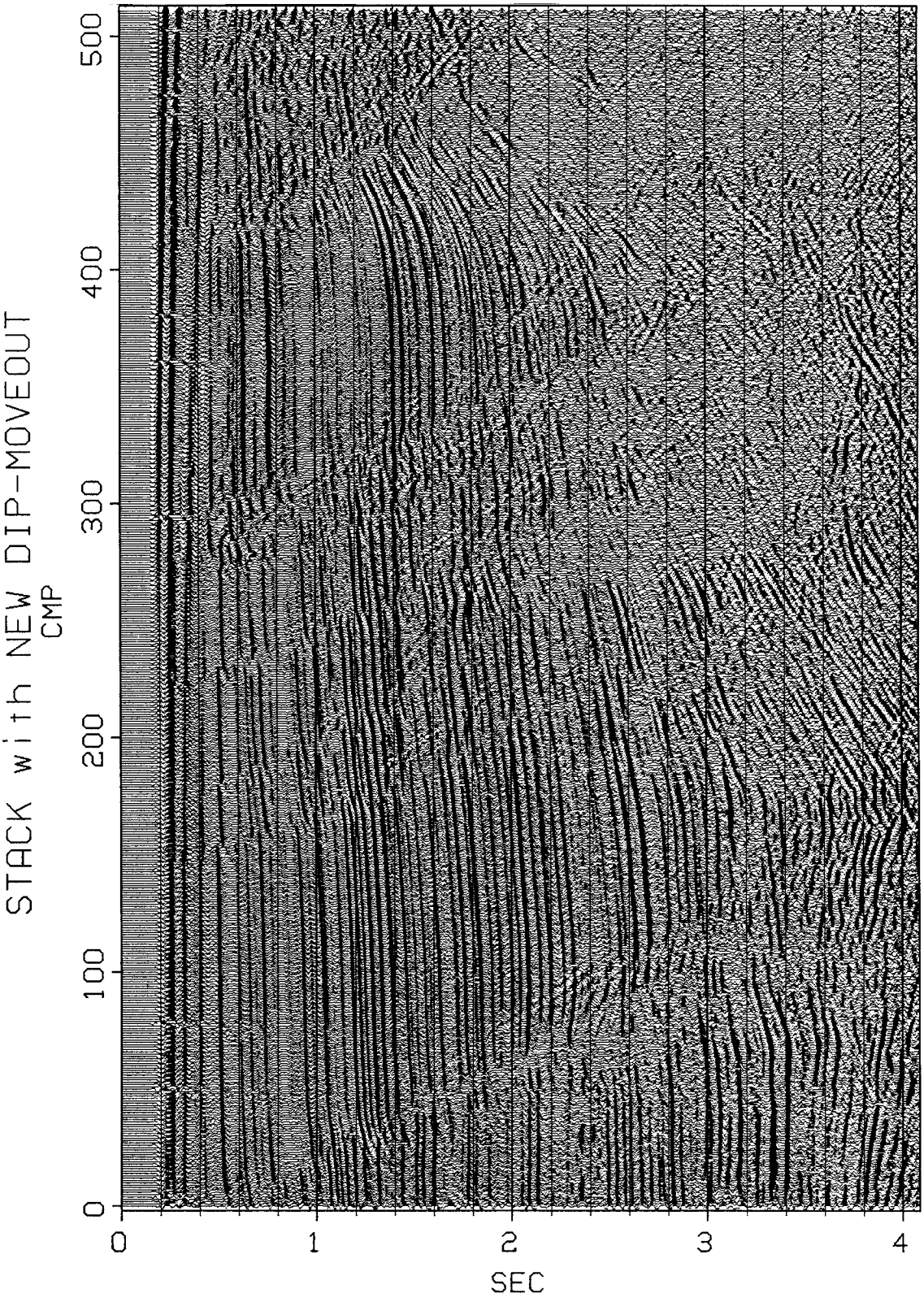

FIG. 2.7a. CMP stack of recorded data, computed using the new DMO algorithm that approximately handles depth-variable velocity. This stack is virtually identical to that plotted in Figure 2.7b, which was obtained using the old constant-velocity algorithm. The CMP interval is 0.033 km.

FIG. 2.7b. CMP stack of recorded data, computed using the old DMO algorithm that was derived assuming constant velocity. This stack is replotted from Figure 1.10a of chapter I. The CMP interval is 0.033 km.

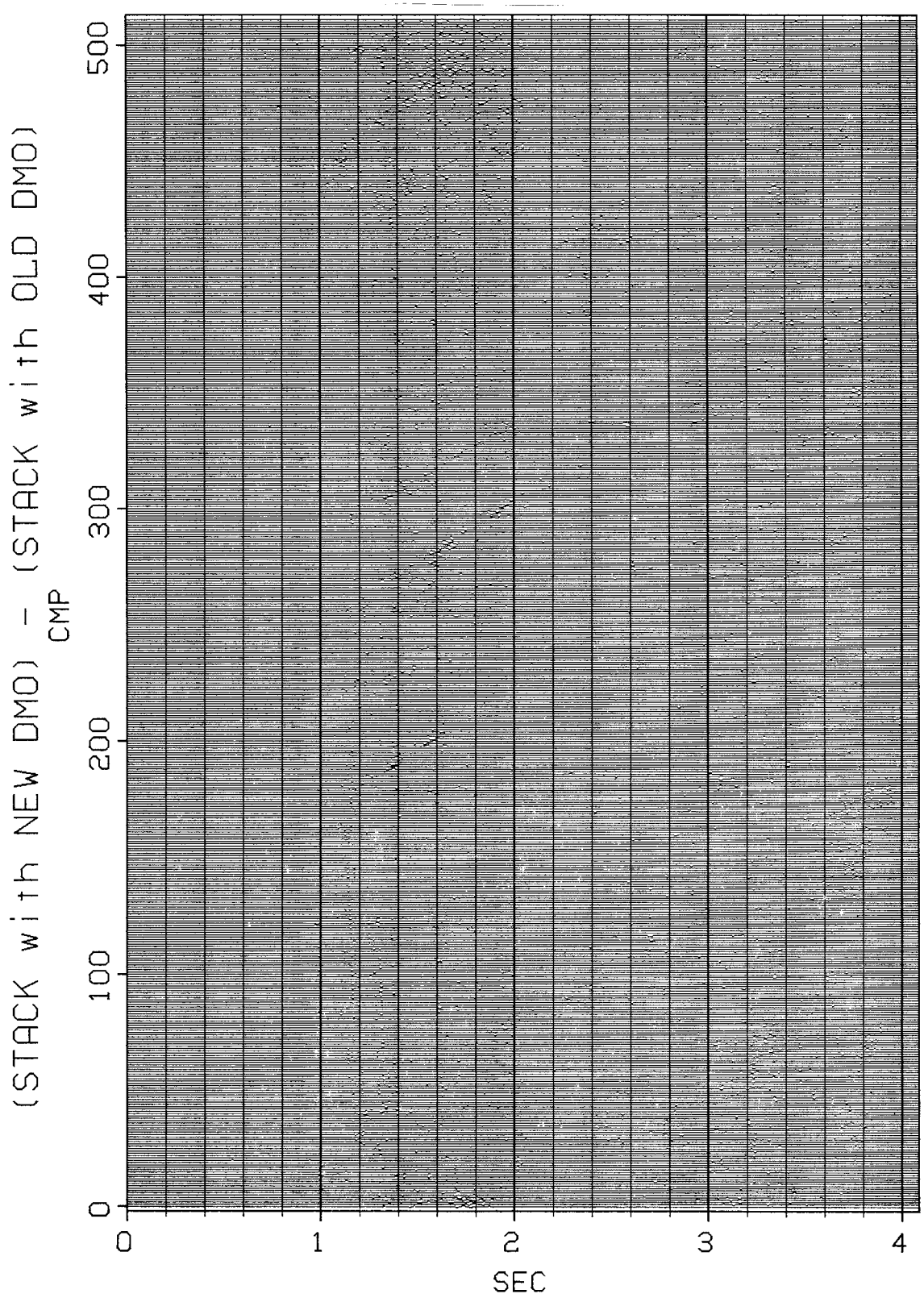

FIG. 2.7c. Figure 2.7b subtracted from Figure 2.7a; i.e., the difference between old and new DMO processing. This difference is insignificant relative to the difference between including or omitting DMO processing. Figures 2.7a, 2.7b, and 2.7c are all plotted with the same gain.

depth-variable velocity may be obtained, at the cost of decreased efficiency.

In practice, the correction for depth-variable velocity, no matter how accurate, is likely to be small compared with the total DMO correction. The relative significance of these corrections was well illustrated by both synthetic and recorded data examples discussed in this chapter. Nevertheless, given any rough estimate of velocity as a function of depth, the new DMO algorithm should be used instead of the old algorithm.